# AniTalker: Animate Vivid and Diverse Talking Faces through Identity-Decoupled Facial Motion Encoding

**Tao Liu**
liutaw@sjtu.edu.cn
X-LANCE Lab, Shanghai Jiao Tong
University
Shanghai, China

**Feilong Chen**
feilong.chen@aispeech.com
AISpeech Ltd
Suzhou, China

**Shuai Fan**
shuai.fan@aispeech.com
AISpeech Ltd
Suzhou, China

**Chenpeng Du**
chenpeng.du@icloud.com
X-LANCE Lab, Shanghai Jiao Tong
University
Shanghai, China

**Qi Chen**
cq1073554383@sjtu.edu.cn
X-LANCE Lab, Shanghai Jiao Tong
University
Shanghai, China

**Xie Chen**
chenxie95@sjtu.edu.cn
X-LANCE Lab, Shanghai Jiao Tong
University
Shanghai, China

**Kai Yu**[*]
kai.yu@sjtu.edu.cn
X-LANCE Lab, Shanghai Jiao Tong
University
Shanghai, China

**Figure 1: We introduce AniTalker, a framework that transforms a single static portrait and input audio into animated talking videos with naturally flowing movements. Each column of generated results utilizes identical control signals with similar poses and expressions but incorporates some random variations, demonstrating the diversity of our generated outcomes.**

## ABSTRACT

The paper introduces AniTalker, an innovative framework designed to generate lifelike talking faces from a single portrait. Unlike existing models that primarily focus on verbal cues such as lip synchronization and fail to capture the complex dynamics of facial expressions and nonverbal cues, AniTalker employs a universal motion representation. This innovative representation effectively captures a wide range of facial dynamics, including subtle expressions and head movements. AniTalker enhances motion depiction through two self-supervised learning strategies: the first involves reconstructing target video frames from source frames within the same identity to learn subtle motion representations, and the second develops an identity encoder using metric learning while actively minimizing mutual information between the identity and motion encoders. This approach ensures that the motion representation is dynamic and devoid of identity-specific details, significantly reducing the need for labeled data. Additionally, the integration of a diffusion model with a variance adapter allows for the generation of diverse and controllable facial animations. This method not only demonstrates AniTalker's capability to create detailed and realistic facial movements but also underscores its potential in crafting dynamic avatars for real-world applications. Synthetic results can be viewed at https://github.com/X-LANCE/AniTalker.

## CCS CONCEPTS

• **Computing methodologies** → **Motion capture**; **Procedural animation**.

## KEYWORDS

Talking Face, Self-supervised, Motion Encoding, Disentanglement

## 1 INTRODUCTION

Integrating speech signals with single portraits [13, 18, 33, 45, 47, 59–61] to generate talking avatars has greatly enhanced both the entertainment and education sectors, providing innovative avenues for interactive digital experiences. While current methodologies [36, 47, 57, 61, 62] have made notable strides in achieving synchronicity between speech signals and lip movements, thus enhancing verbal communication, they often neglect the critical aspect of nonverbal communication. Nonverbal communication encompasses the transmission of information without the use of words, including but not limited to specific head movements, facial expressions, and blinking. Research [35] indicates that these nonverbal cues are pivotal in communicating.

The primary challenge lies in the inadequacy of existing models to encapsulate the complex dynamics associated with facial motion representation. Existing approaches predominantly employ explicit structural representations such as blendshapes [3, 13, 34], landmark coefficients [18, 48, 60], or 3D Morphable Models (3DMM) [7, 14, 27] to animate faces. Designed initially for single-image processing, these methods offer a constrained approximation of facial dynamics, failing to capture the full breadth of human expressiveness. Recent advancements [11, 25] have introduced trainable facial motion encoders as alternatives to conventional explicit features, showing

significant progress in capturing detailed facial movements. However, their deployment is often tailored for specific speakers [11] or limited to the mouth region [25], highlighting a gap in fine-grained motion representation that captures all varieties of facial dynamics.

A universal and fine-grained motion representation that is applicable across different characters remains absent. Such a representation should fulfill three key criteria: capturing minute details, such as minor mouth movements, eye blinks, or slight facial muscle twitching; ensuring universality, making it applicable to any speaker while removing identity-specific information to maintain a clear separation between appearance and motion; and incorporating a wide range of nonverbal cues, such as expressions, head movements, and posture.

In this paper, we introduce **AniTalker**. Our approach hinges on a universal motion encoder designed to grasp the intricacies of facial dynamics. By adopting the self-supervised learning paradigm, we mitigate the reliance on labeled data, enabling our motion encoder to learn robust motion representations. This learning process operates on dual levels: one entails understanding motion dynamics through the transformation of a source image into a target image, capturing a spectrum of facial movements, from subtle changes to significant alterations. Concurrently, the use of identity labels within the dataset facilitates the joint optimization of an identity recognition network in a self-supervised manner, further aiming to disentangle identity from motion information through mutual information minimization. This ensures that the motion representation retains minimal identity information, upholding its universal applicability.

To authenticate the versatility of our motion space, we integrate a diffusion model and a variance adapter to enable varied generation and manipulation of facial animations. Thanks to our sophisticated representation and the diffusion motion generator, AniTalker is capable of producing diverse and controllable talking faces.

In summary, our contributions are threefold:

(1) We have developed universal facial motion encoders using a self-supervised approach that effectively captures facial dynamics across various individuals. These encoders feature an identity decoupling mechanism to minimize identity information in the motion data and prevent identity leakage.

(2) Our framework includes a motion generation system that combines a diffusion-based motion generator with a variance adapter. This system allows for the production of diverse and controllable facial animations, showcasing the flexibility of our motion space.

(3) Extensive evaluations affirm our framework's contribution to enhancing the realism and dynamism of digital human representations, while simultaneously preserving identity.

## 2 RELATED WORKS

**Speech-driven Talking Face Generation** refers to creating talking faces driven by speech, We categorize the models based on whether they are single-stage or two-stage. Single-stage models [36, 58, 61] generate images directly from speech, performing end-to-end rendering. Due to the size constraints of rendering networks, this method struggles with processing longer videos, generally managing hundreds of milliseconds. The two-stage type [3, 11, 13,

---
*The Corresponding author.

18, 25, 33, 60] decouples motion information from facial appearance and consists of a speech-to-motion generator followed by a motion-to-video rendering stage. As the first stage solely generates motion information and does not involve the texture information of the frames, it requires less model size and can handle long sequences, up to several seconds or even minutes. This two-stage method is known to reduce jitter [3, 11, 25], enhance speech-to-motion synchronization [11, 13, 33, 60], reduce the need for aligned audio-visual training data [3, 25], and enable the creation of longer videos [18]. Our framework also employs a two-stage structure but with a redesigned motion representation and generation process.

**Motion Representation** serves as an essential bridge between the driving features and the final rendered output in creating talking faces. Current methods predominantly utilize explicit structural representations, such as blendshapes [3, 13, 32], 3D Morphable Models (3DMMs) [27], or landmarks [48, 60]. These formats offer high interpretability and facilitate the separation of facial actions from textures, making them favored as intermediary representations in facial generation tasks. However, due to the wide range of variability in real-world facial movements, they often fail to capture the subtle nuances of facial expressions fully, thus limiting the diversity and expressiveness of methods dependent on these representations. Our research is dedicated to expanding the spectrum of motion representation by developing a learned implicit representation that is not constrained by the limitations of explicit parametric models.

**Self-supervised motion transfer approaches** [31, 41, 44, 48, 49, 51, 54] aim to reconstruct the target image from a source image by learning robust motion representations from a large amount of unlabeled data. This significantly reduces the need for labeled data. A key challenge in these methods is separating motion from identity information. They primarily warp the source image using predicted dense optical flow fields. This approach attempts to disentangle motion from identity by predicting distortions and transformations of the source image. However, information leakage occurs in practice, causing the target image to contain not just motion but also identity information. Building on this observation, we explicitly introduce identity modeling and employ the Mutual Information Neural Estimation (MINE) [1, 4] method to achieve a motion representation independent of identity.

**Diffusion Models** [19] have demonstrated outstanding performance across various generative tasks [12, 17, 21, 39]. Recent research has utilized diffusion models as a rendering module [2, 11, 25, 29, 40, 43, 45]. Although diffusion models often produce higher-quality images, they require extensive model parameters and substantial training data to converge. To enhance the generation process, several approaches [18, 27, 28, 32, 55] employ diffusion models for generating motion representations. Diffusion models excel at addressing the one-to-many mapping challenge, which is crucial for speech-driven generation tasks. Given that the same audio clip can lead to different actions (e.g., lip movements and head poses) across different individuals or even within the same person, diffusion models provide a robust solution for managing this variability. Additionally, the training and inference phases of diffusion models, which systematically introduce and then remove noise, allow for the incorporation of noise during generation to foster diversity. We also use diffusion in conjunction with our motion

representation to further explore diversity in talking face generation.

## 3 ANITALKER FRAMEWORK

### 3.1 Model Overview

AniTalker contains two critical components: (1) Training a motion representation that can capture universal face dynamics, and (2) Based on the well-trained motion encoder from the previous step, the generation or manipulation of the motion representation using the user-controlled driving signal to produce the synthesised talking face video.

### 3.2 Universal Motion Representation

Our approach utilizes a self-supervised image animation framework, employing two RGB images from a video clip: a source image $I^s$ and a target image $I^t$ ($I \in \mathbb{R}^{H \times W \times 3}$), to serve distinct functions: $I^s$ provides identity information, whereas $I^t$ delivers motion details. The primary aim is to reconstruct $I^t$. Due to the random selection of frames, occasionally adjacent frames are chosen, enabling the network to learn representations of subtle movements. As depicted in Figure 2 (a), both the source and target images originate from the same video clip. Through this self-supervised learning method, the target image's encoder is intended to exclusively capture motion information. By learning from frame-to-frame transfer, we can acquire a more universal representation of facial motion. This representation includes verbal actions such as lip movements, as well as nonverbal actions, including expressions, posture, and movement.

To explicitly decouple motion and identity in the aforementioned processes, we strengthen the self-supervised learning approach by incorporating Metric Learning (ML) and Mutual Information Disentanglement (MID). Specifically:

**Metric Learning.** Drawing inspiration from face recognition [8, 46] and speaker identification [9], metric learning facilitates the generation of robust identity information. This technique employs a strategy involving pairs of positive and negative samples, aiming to minimize the distance between similar samples and maximize it between dissimilar ones, thereby enhancing the network's ability to discriminate between different identities. This process can also proceed in a self-supervised fashion, with each iteration randomly selecting distinct identities from the dataset. Specifically, the approach establishes an anchor ($a$) and selects a positive sample ($p$) and a negative sample ($n$)—corresponding to faces of different identities—with the goal of reducing the distance ($d$) between the anchor and the positive sample while increasing the distance between the anchor and the negative samples. This optimization, depicted in Figure 2 (b), involves randomly selecting a different identity from a list of candidates not belonging to the current person as the negative sample. The optimization goal for this process is as follows:

$$\mathcal{L}_{ML} = \max\left(0,\ d(a, p) - d(a, n) + \text{margin}\right)$$

Here, the margin is a positive threshold introduced to further separate the positive and negative samples, thus improving the model's ability to distinguish between different identities.

**Mutual Information Disentanglement.** Although metric learning effectively constrains the identity encoder, focusing solely on this encoder does not adequately minimize the identity information
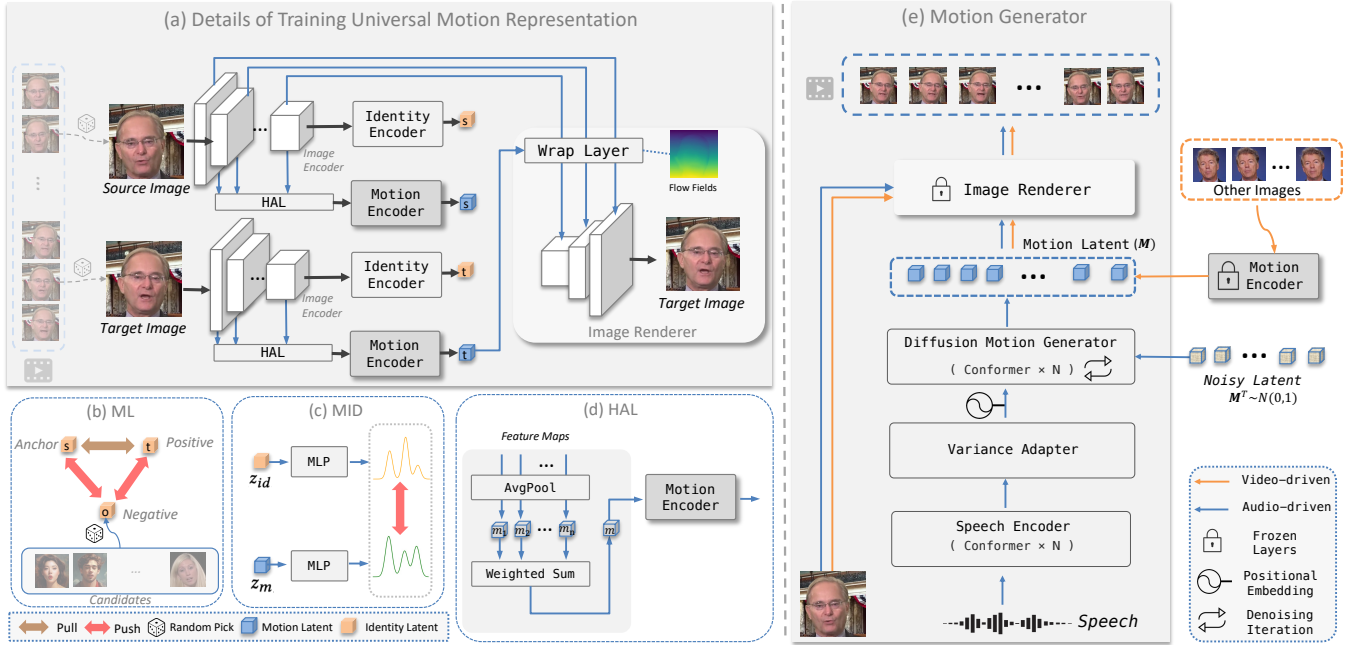
**Figure 2: The AniTalker framework comprises two main components: learning a universal motion representation and then generating and manipulating this representation through a sequence model. Specifically, the first part aims to learn a robust motion representation by employing metric learning (ML), mutual information disentanglement (MID), and Hierarchical Aggregation Layer (HAL). Subsequently, this motion representation can be used for further generation and manipulation.**

within the motion encoder. To tackle this issue, we utilize Mutual Information (MI), a statistical measure that evaluates the dependency between the outputs of the identity and motion encoders. Given the challenge of directly computing MI between two variables, we adopt a parametric method to approximate MI estimation among random variables. Specifically, we use CLUB [4], which estimates an upper bound for MI. Assuming the output of the identity encoder is the identity latent $z_{id}$ and the motion encoder's output is the motion latent $z_m$, our goal is to optimize the mutual information $I(\mathcal{E}(z_{id}); \mathcal{E}(z_m))$, where $\mathcal{E}$ denotes the learnable Multi-Layer Perceptron (MLP) within CLUB. This optimization ensures that the motion encoder primarily captures motion, thereby preventing identity information from contaminating the motion space. This strategy is depicted in Figure 2 (c).

In summary, by leveraging Metric Learning and Mutual Information Disentanglement, we enhance the model's capacity to accurately differentiate between identity and motion while reducing reliance on labeled data.

**Hierarchical Aggregation Layer (HAL).** To enhance the motion encoder's capability to understand motion variance across different scales, we introduce the Hierarchical Aggregation Layer (HAL). This layer aims to integrate information from various stages of the image encoder, each providing different receptive fields [24]. HAL processes inputs from all intermediate layers of the image encoder and passes them through an Average Pooling (AvgPool) layer to capture scale-specific information. A Weighted Sum [53] layer follows, assigning learnable weights to effectively merge information from these diverse layers. This soft fusion approach enables the

motion encoder to capture and depict movements across a broad range of scales. Such a strategy allows our representations to adapt to faces of different sizes without the need for prior face alignment or normalization.

Specifically, the features following the AvgPool layer are denoted as $[m_1, m_2, \ldots, m_n]$, representing the set of averaged features, with $[w_1, w_2, \ldots, w_n]$ as the corresponding set of weights, where $n$ symbolizes the number of intermediate layers in the image encoder. These weights undergo normalization through the softmax function to guarantee a cumulative weight of 1. The equation for the weighted sum of tensors, indicating the layer's output, is formulated as $\mathbf{m} = \sum_{i=1}^{n} w_i \cdot m_i$. The softmax normalization process is mathematically articulated as $w_i = \frac{e^{W_i}}{\sum_{j=1}^{n} e^{W_j}}$, ensuring the proportional distribution of weights across the various layers. Subsequently, $\mathbf{m}$ is fed into the motion encoder for further encoding.

**Learning Objective.** The main goal of learning is to reconstruct the target image by inputting two images: the source and the target within the current identity index. Several loss functions are utilized during the training process, including reconstruction loss $L_{recon}$, perceptual loss $L_{percep}$, adversarial loss $L_{adv}$, mutual information loss $L_{MI}$, and identity metric learning loss $L_{ML}$. The total loss is formulated as follows:

$$L_{motion} = L_{recon} + \lambda_1 L_{percep} + \lambda_2 L_{adv} + \lambda_3 L_{MI} + \lambda_4 L_{ML}$$

## 3.3 Motion Generation

Once the motion encoder and image renderer are trained, at the second stage, we can freeze these models. The motion encoder is used to generate images, then video-driven or speech-driven methods are employed to produce motion, and finally, the image renderer carries out the final frame-by-frame rendering.

*3.3.1 Video-Driven Pipeline.* Video driving, also referred to face reenactment, leverages a driven speaker's video sequence $\mathbf{I}^d = [I_1^d, I_2^d, \ldots, I_T^d]$ to animate a source image $I^s$, resulting in a video that accurately replicates the driven poses and facial expressions. In this process, the video sequence $\mathbf{I}^d$ is input into the motion encoder, previously trained in the first phase, to extract the motion latent. This latent, along with $I^s$, is then directly fed, frame by frame, into the image renderer for rendering. No additional training is required. The detailed inference process, where the orange lines represent the data flow during video-driven inference, is depicted in Figure 2 (e).

*3.3.2 Speech-Driven Pipeline.* Unlike video-driven methods that use images, the speech-driven approach generates videos consistent with the speech signal or other control signals to animate a source image $I^s$. Specifically, we utilize a combination of diffusion and variance adapters: the former learns a better distribution of motion data, while the latter mainly introduces attribute manipulation.

**Diffusion Models.** For generating motion latent sequences, we utilize a multi-layer Conformer [16]. During training, we incorporate the training process of diffusion, which includes both adding noise and denoising steps. The noising process gradually converts clean Motion Latent $\mathbf{M}$ into Gaussian noise $\mathbf{M}^T$, where $T$ represents the number of total denoising steps in the diffusion process. Conversely, the denoising process systematically eliminates noise from the Gaussian noise, resulting in clean Motion Latents. This iterative process better captures the distribution of motion, enhancing the diversity of the generated results. During the training phase, we adhere to the methodology described in [19] for the DDPM's training stage, applying the specified simplified loss objective, as illustrated in Equation 1, where $t$ represents a specific time step and $\mathbf{C}$ represents the control signal, which refers to either speech or speech perturbed by a Variance Adapter (to be discussed in the following section). For inference, considering the numerous iteration steps required by diffusion, we select the Denoising Diffusion Implicit Model (DDIM) [42]—an alternate non-Markovian noising process—as the solver to quicken the sampling process.

$$L_{\text{diff}} = \mathbb{E}_{t,\mathbf{M},\epsilon} \left[ \|\epsilon - \hat{\epsilon}_t \left( \mathbf{M}_t, t, \mathbf{C} \right)\|^2 \right] \quad (1)$$

**Variance Adapter.** The Variance Adapter [38] is a residual branch connected to audio features, allowing optional control over the speech signal. Originally proposed to mitigate the one-to-many problem in Text-to-Speech (TTS) tasks, its architecture includes a predictor and an encoder that use speech signals to predict attribute representations. A residual connection is then applied between the encoder output and the speech signals. During the Training Stage, the encoder processes speech features in collaboration with the predictor to minimize the L2 loss against a ground truth control signal. This includes incorporating an attribute extractor for targeting specific attributes, such as employing a pose extractor (yaw, pitch, roll) to control head posture during the audio generation process. In
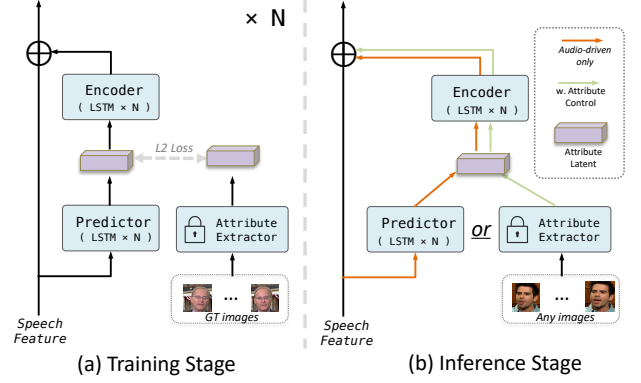


**Figure 3: Variance Adapter Block. Each block models a single attribute and can be iterated multiple times, where $N$ represents the number of attributes.**

the Inference Stage, the trained encoder and predictor can flexibly synthesize speech with controlled attributes or operate based on speech-driven inputs. The detailed structure is depicted in Figure 3. Our approach extends previous works [11, 18] by incorporating LSTM [15] for improved temporal modeling and introducing additional cues such as head position and head scale, which we refer to as camera parameters. The architecture is detailed in Figure 3.

**Learning Objective.** The total loss comprises diffusion loss and variance adapter loss, where $K$ represents the number of attributes:

$$L_{\text{gen}} = L_{\text{diff}} + \lambda \sum_{k=1}^{K} L_{\text{var}_k}$$

## 4 EXPERIMENTS

### 4.1 Experimental Settings

We utilizes three datasets: VoxCeleb [30], HDTF [59], and VFHQ [52]. Due to different processing approaches across these datasets, we re-downloaded the original videos and processed them in a unified way. Specifically, our processing pipeline included filtering out blurred faces and faces at extreme angles. It is noted that we did not align faces but instead used a fixed detection box for each video clip, allowing for natural head movement. This effort resulted in a dataset containing 4,242 unique speaker IDs, encompassing 17,108 video clips with a cumulative duration of 55 hours. Details of this filtering process are provided in the supplementary material. Each video in these datasets carries a unique facial ID tag, which we used as labels for training our identity encoder. We also reserved some videos from HDTF for testing, following the test split in [58].

**Scenario Setting** We evaluate methods under two scenarios: video-driven and speech-driven, both operating on a one-shot basis with only a single portrait required. The primary distinction lies in the source of animation: image sequences for video-driven and audio signals for speech-driven scenarios. The detailed data flow for inference is illustrated in Figure 2. Additionally, each scenario is divided into two types: self-driven, where the source and target

share the same identity, and cross-driven, involving different identities. In speech-driven tasks, if posture information is needed, it is provided from the ground truth. Moreover, for our motion generator, unless specified otherwise, we use a consistent seed to generate all outcomes. To ensure a fair comparison, the output resolution for all algorithms is standardized to $256 \times 256$.

**Implementation Details** In training the motion representation, our self-supervised training paradigm is primarily based on LIA [49]. Both the identity and motion encoders employ MLPs. Our training targets use the CLUB [1] for mutual information loss, in conjunction with AAM-Softmax [46]. This robust metric learning method utilizes angular distance and incorporates an increased number of negative samples to enhance the metric learning loss. In the second phase, the speech encoder and the Motion Generator utilize a four-layer and a two-layer conformer architecture, respectively, inspired by [11, 25]. This architecture integrates the conformer structure [16] and relative positional encoding [6]. A pre-trained HuBERT-large model [20] serves as the audio feature encoder, incorporating a downsampling layer to adjust the audio sampling rate from 50 Hz to 25 Hz to synchronize with the video frame rate. The training of the audio generation process spans 125 frames (5 seconds). Detailed implementation specifics and model structure are further elaborated in the supplementary materials.

**Evaluation Metric** For **objective metrics**, we utilize Peak Signal-to-Noise Ratio (PSNR), Structural Similarity Index (SSIM) [50], and Learned Perceptual Image Patch Similarity (LPIPS) [56] to quantify the similarity between generated and ground truth images. Cosine Similarity (CSIM) [2] measures facial similarity using a pretrained face recognition. Lip-sync Error Distance (LSE-D) [5] assesses the alignment between generated lip movements and the corresponding audio. Regarding **subjective metrics**, we employ the Mean Opinion Score (MOS) as our metric, with 10 participants rating our method based on Fidelity (F), Lip-sync (LS), Naturalness (N), and Motion Jittering (MJ).

## 4.2 Video Driven Methods

**Table 1: Quantitative comparisons with previous Face Reenactment methods.**

| Method | Self-Reenactment | | | | Cross-Reenactment | | |
|---|---|---|---|---|---|---|---|
| | PSNR↑ | SSIM↑ | LPIPS↓ | CSIM↑ | SSIM↑ | LPIPS↓ | CSIM↑ |
| FOMM [41] | 23.944 | 0.775 | 0.178 | 0.830 | 0.411 | 0.423 | 0.494 |
| DPE [31] | 27.239 | 0.861 | 0.151 | 0.912 | 0.445 | 0.410 | 0.567 |
| MTIA [44] | 28.435 | 0.870 | 0.122 | **0.929** | 0.393 | 0.456 | 0.448 |
| Vid2Vid [48] | 27.659 | 0.870 | 0.115 | 0.924 | 0.410 | 0.401 | 0.553 |
| LIA [49] | 25.854 | 0.831 | 0.137 | 0.916 | 0.421 | 0.406 | 0.522 |
| FADM [54] | 26.169 | 0.849 | 0.147 | 0.916 | 0.445 | 0.399 | 0.574 |
| **AniTalker** | **29.071** | **0.905** | **0.079** | 0.927 | **0.494** | **0.347** | **0.586** |

**Quantitative Results** We benchmarked our approach against several leading face reenactment methods [31, 41, 44, 48, 49, 54], all employing variations of self-supervised learning. The results are presented in Table 1. Due to the inherent challenges and the absence

of frame-by-frame ground truth in Cross-Reenactment (using another person's video for driving), the overall results tend to be lower compared to Self-Reenactment (using the current person's video). In Self-Reenactment, our algorithm achieved superior results for image structural metrics such as PSNR, SSIM, and LPIPS, validating the effectiveness of our motion representation in reconstructing images. Additionally, using the CSIM metric to measure face similarity, we observed that the similarity between the reconstructed face and the original portrait was the second highest, slightly behind MTIA [44], illustrating our model's identity preservation capabilities. For Cross-Reenactment, where the portrait serves as ground truth and considering cross-driven deformations, we focused on high-level metrics: SSIM and LPIPS. Our method demonstrated commendable performance. We also evaluated CSIM, which, unlike self-reenactment, showed a significant improvement, achieving the best results among these datasets. This highlights our algorithm's outstanding ability to disentangle identity and motion when driving with different individuals.

**Qualitative Results** To highlight comparative results, we conducted a cross-reenactment scenario analysis with different algorithms, as presented in Figure 4. The objective was to deform the source portrait using the actions of the target. Each row in the figure represents a driving case. We observed that baseline methods exhibited varying degrees of identity leakage, where the identity information from the target contaminated the source portrait's identity. For example, as demonstrated in the fourth row, the slim facial structure of the driving portrait led to slimmer outcomes, which was unintended. However, our results consistently preserved the facial identity. Additionally, in terms of expression recovery, as evident in the first and third rows, our approach replicated the action of opening the eyes in the source portrait accurately, creating a natural set of eyes. In contrast, other algorithms either produced slight eye-opening or unnatural eyes. These qualitative findings highlight the advantage of decoupling ability.

## 4.3 Speech-driven Methods

**Table 2: Quantitative comparisons with previous speech-driven methods. The subjective evaluation is the mean option score (MOS) rated at five grades (1-5) in terms of Fidelity (F), Lip-Sync (LS), Naturalness (N), and Motion Jittering (MJ).**

| Method | Subjective Evaluation | | | | Objective Evaluation (Self) | | |
|---|---|---|---|---|---|---|---|
| | MOS-F↑ | MOS-LS↑ | MOS-N↑ | MOS-MJ↑ | SSIM↑ | CSIM↑ | Sync-D↓ |
| MakeItTalk [62] | 3.434 | 1.922 | 2.823 | 3.129 | 0.580 | 0.719 | 8.933 |
| PC-AVS [61] | 3.322 | 3.785 | 2.582 | 2.573 | 0.305 | 0.703 | **7.597** |
| Audio2Head [47] | 3.127 | 3.650 | 2.891 | 2.467 | 0.597 | 0.719 | 8.197 |
| SadTalker [57] | 3.772 | 3.963 | 2.733 | 3.883 | 0.504 | 0.723 | 7.967 |
| **AniTalker** | **3.832** | **3.978** | **3.832** | **3.976** | **0.671** | **0.725** | 8.298 |

We compare our method against existing state-of-the-art speech-driven approaches, including MakeItTalk [62], PC-AVS [61], Audio2Head [47], and SadTalker [57]. **Quantitative results** are presented in Table 2. From the subjective evaluation, our method consistently shows improvements in fidelity, lip-sync accuracy, naturalness, and a reduction in motion jittering, particularly noted for the enhanced naturalness of movements. These advancements can

---

[1]https://github.com/Linear95/CLUB/
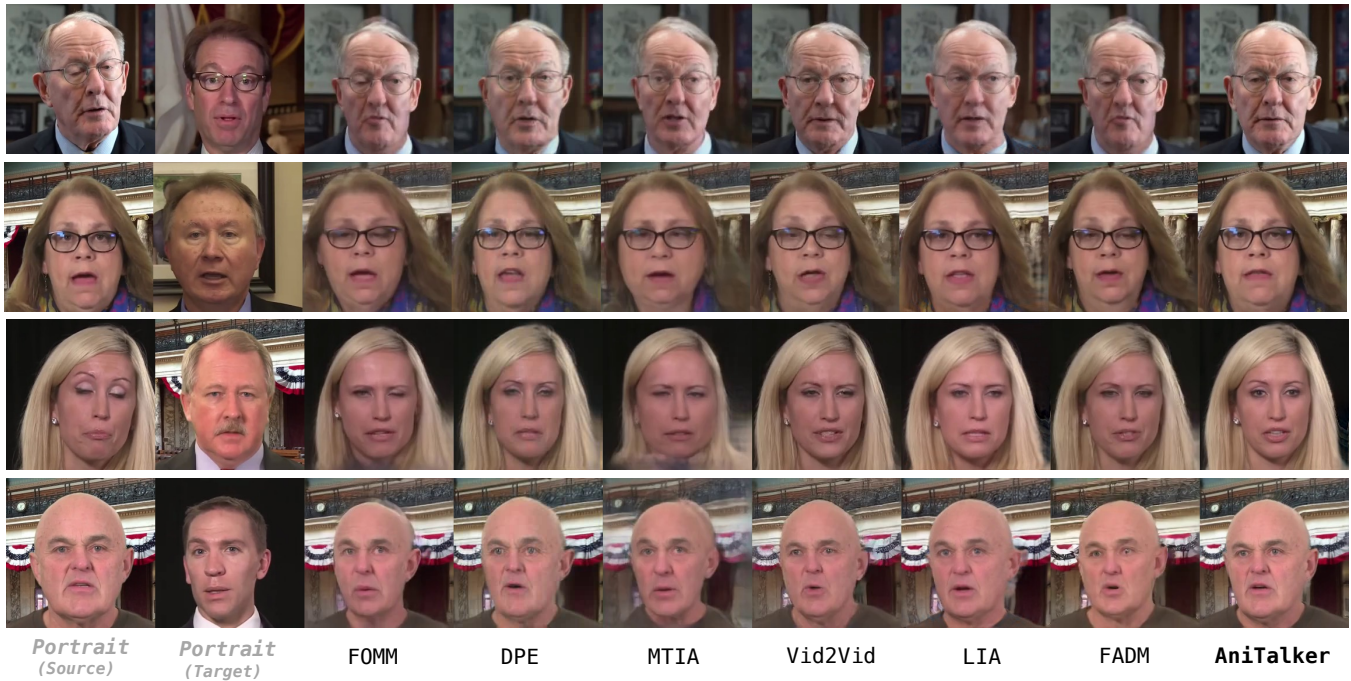[2]https://github.com/dc3ea9f/vico_challenge_baseline

**Figure 4: Cross-Reenactment Visualization: This task involves transferring actions from a target portrait to a source portrait to evaluate each algorithm's ability to separate motion and appearance. Starting from the third column, each column represents the output from a different algorithm. The results highlight our method's superior ability to preserve fidelity in both motion transfer and appearance retention.**
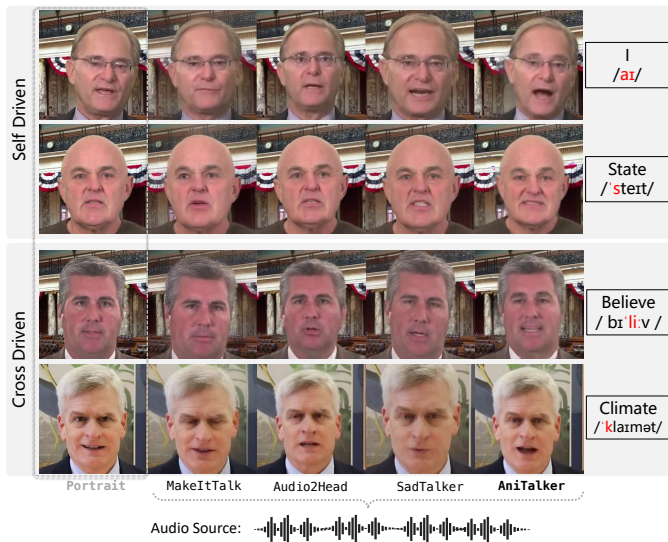


**Figure 5: Visual comparison of the speech-driven method in self- and cross-driven scenarios. Phonetic sounds are highlighted in red.**

be attributed to our sophisticated universal motion representation. The objective evaluation involves driving the image with its audio.

Compared to these methods, our approach shows significant improvements in SSIM and CSIM. However, our Sync-D metric shows a decrease, which we believe is due to two main reasons: (1) we do not use this metric as a supervisory signal, and (2) the Sync-D metric focuses on short-term alignment and does not adequately represent long-term information that is more crucial for the comprehensibility of generated videos. This is also corroborated by the **qualitative results** shown in Figure 5, highlighting our model's ability to produce convincingly synchronized lip movements to the given phonetic sounds.

## 4.4 Ablation Study

**Table 3: Quantitative comparisons of disentanglement methods and the HAL module in Self-Reenactment setting**

| Method | ML | MID | HAL | PNSR ↑ | SSIM ↑ | CSIM ↑ |
|---|---|---|---|---|---|---|
| Baseline | | | | 25.854 | 0.849 | 0.916 |
| Triplet [10] | ✓ | | | 26.455 | 0.860 | 0.911 |
| AAM-Softmax [46] | ✓ | | | 27.922 | 0.894 | 0.923 |
| AAM-Softmax + CLUB [4] | ✓ | ✓ | | 28.728 | 0.900 | 0.924 |
| **AniTalker** | ✓ | ✓ | ✓ | **29.071** | **0.905** | **0.927** |

*4.4.1 Ablations on Disentanglement.* To further validate the effectiveness of our disentanglement between motion and identity, we

conducted tests using various methods. Initially, to evaluate the performance of developing a reliable identity encoder using only Metric Learning (ML) without Mutual Information Disentanglement (MID), we assessed both Triplet loss [10] and AAM-Softmax [46]. Our results indicate that AAM-Softmax, an angle-based metric, achieves superior outcomes in our experiments. Additionally, by incorporating a mutual information decoupling module alongside AAM-Softmax, we noted further improvements in results. This enhancement encouraged the motion encoder to focus exclusively on motion-related information. These findings are comprehensively detailed in Table 3.

**Table 4: Different intermediate representations under the Self-Reenactment setting. 'Face Repr.' is short for face representation, and 'Dim.' represents the corresponding dimension.**

| Method | Face Repr. | Dim. | PSNR ↑ | SSIM ↑ | CSIM↑ |
|---|---|---|---|---|---|
| EMOCA [7] | 3DMM | 50 | 20.911 | 0.670 | 0.768 |
| PIPNet [22] | Landmark | 136 | 22.360 | 0.725 | 0.830 |
| **AniTalker** | Motion Latent | 20 | **29.071** | **0.905** | **0.927** |

*4.4.2 Ablation Study on Motion Representation.* To compare our motion representation with commonly used landmark and 3D Morphable Model (3DMM) representations, we utilized 68 2D coordinates [22] (136 dimensions) for the landmark representation and expression parameters (50 dimensions) from EMOCA [7] for the 3DMM representation. In self-reenactment scenarios, all rendering methods were kept consistent, and different features were used to generate driven images. We observed several key points: (1) As shown in Table 4, our learned representation exhibits a more compact dimensionality, indicating a more succinct encoding of facial dynamics. (2) Our video comparisons show that, unlike these explicit representations, our implicit motion representation maintains frame stability without the need for additional smoothing. This can be attributed to our self-supervised training strategy of sampling adjacent frames, which effectively captures subtle dynamic changes while inherently ensuring temporal stability.
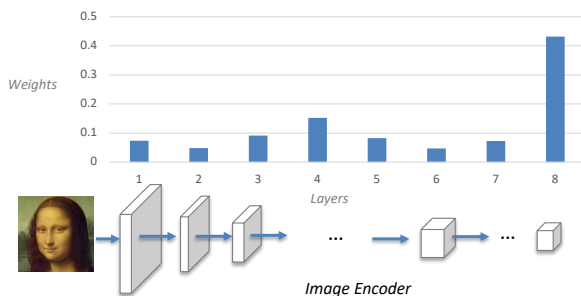


**Figure 6: The weights of motion representation from different layers of the Image Encoder.**

*4.4.3 Ablations on HAL.* To explore the significance of the Hierarchical Aggregation Layer (HAL) in dynamic representations, we conducted a series of ablation experiments focusing on the HAL layer. The results showed that models incorporating the HAL layer exhibited performance improvements, as detailed in the final row of Table 3. To analyze the impact and importance of different HAL layers on motion representation, we extracted and examined the softmax-normalized weights of each layer (a total of 8 layers in our experiment) in our Image Encoder as shown in Figure 6. It was found that the weights of the last layer contributed most significantly, likely because it represents global features that can effectively recover most motion information. Notably, the fourth layer—situated in the middle of the image encoder feature map—demonstrated a local maximum. Considering the receptive field size of this layer's patch is similar to the size of eyes and approximately half the size of the mouth, this finding suggests that the layer plays a potential role in simulating areas such as the mouth and eyes. These results not only confirm the pivotal role of the HAL layer in dynamic representation but also reveal the deep mechanisms of the model's ability to capture facial movements of different scales.
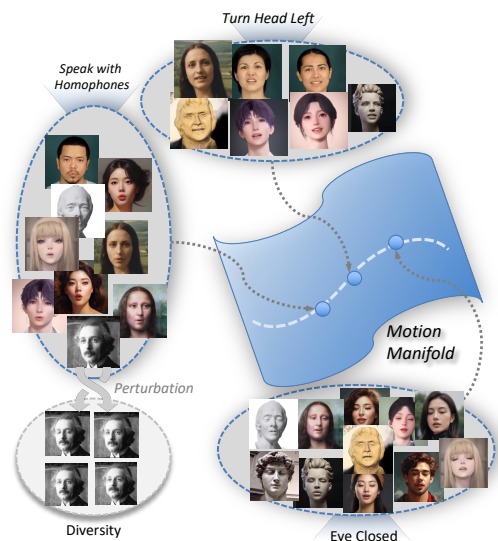


**Figure 7: Motion Manifold of the continuous motion space.**

## 5 DISCUSSION

**Discussion on Universal Motion Representation** Our investigations into the model's ability to encode facial dynamics have highlighted a universal representation of human facial movements. As depicted in Figure 7, we observed that different individuals maintain consistent postures and expressions (such as turning the head left, speaking with homophones, and closing eyes) at each point within our motion space, demonstrating that our motion space forms a Motion Manifold. This manifold facilitates the representation of a continuous motion space, enabling the precise modeling of subtle facial feature variations and allowing for smooth transitions. Additionally, by integrating perturbations through diffusion noise,

our model can simulate random, minute motion changes that align with fundamental movement patterns, thus enhancing the diversity of generated expressions. These findings demonstrate that our motion representation has a robust capacity to capture and represent a wide array of human facial movements.

**Discussion on Generalization Ability** Although our model is trained on real human faces, it demonstrates the ability to generalize to other images with facial structures, such as cartoons, sculptures, reliefs, and game characters. This underscores the model's excellent scalability. We primarily attribute this capability to the complete decoupling of identity and motion, which ensures that the model grasps the intrinsic nature of facial movements, thereby enhancing its generalization capability.

## 6 CONCLUSION

The AniTalker framework represents a significant advancement in the creation of lifelike talking avatars, addressing the need for a fine-grained and universal motion representation in digital human animation. By integrating a self-supervised universal motion encoder and employing sophisticated techniques like metric learning and mutual information disentanglement, AniTalker effectively captures the subtleties of both verbal and non-verbal facial dynamics. The resulting framework not only achieves enhanced realism in facial animations but also demonstrates strong generalization capabilities across different identities and media. AniTalker sets a new benchmark for the realistic and dynamic representation of digital human faces, promising broad applications in entertainment, communication, and education.

**Limitation and Future Work** While AniTalker shows promise in generalizing motion dynamics, it still faces challenges. Our rendering network generates frames individually, which can lead to inconsistencies in complex backgrounds. Additionally, limited by the performance of the warping technique, extreme cases where the face shifts to a large angle may result in noticeable blurring at the edges. Future work will focus on improving the temporal coherence and rendering effects of the rendering module.

## REFERENCES

[1] Mohamed Ishmael Belghazi, Aristide Baratin, Sai Rajeswar, Sherjil Ozair, Yoshua Bengio, Aaron Courville, and R Devon Hjelm. 2018. Mutual Information Neural Estimation. In *International Conference on Machine Learning (ICML) (Proceedings of Machine Learning Research, Vol. 80)*, Jennifer Dy and Andreas Krause (Eds.). PMLR, 531–540.

[2] Dan Bigioi, Shubhajit Basak, Michał Stypułkowski, Maciej Zieba, Hugh Jordan, Rachel McDonnell, and Peter Corcoran. 2024. Speech driven video editing via an audio-conditioned diffusion model. *Image and Vision Computing* 142 (2024), 104911.

[3] Qi Chen, Ziyang Ma, Tao Liu, Xu Tan, Qu Lu, Kai Yu, and Xie Chen. 2023. Improving few-shot learning for talking face system with tts data augmentation. In *ICASSP 2023-2023 IEEE International Conference on Acoustics, Speech and Signal Processing (ICASSP)*. IEEE, 1–5.

[4] Pengyu Cheng, Weituo Hao, Shuyang Dai, Jiachang Liu, Zhe Gan, and Lawrence Carin. 2020. Club: A contrastive log-ratio upper bound of mutual information. In *International Conference on Machine Learning (ICML)*. PMLR, 1779–1788.

[5] Joon Son Chung and Andrew Zisserman. 2017. Out of time: automated lip sync in the wild. In *Asian Conference on Computer Vision (ACCV) Workshops*.

[6] Zihang Dai, Zhilin Yang, Yiming Yang, Jaime Carbonell, Quoc V Le, and Ruslan Salakhutdinov. 2019. Transformer-xl: Attentive language models beyond a fixed-length context. *Proceedings of the 57th Annual Meeting of the Association for Computational Linguistics* (2019).

[7] Radek Daněček, Michael J Black, and Timo Bolkart. 2022. Emoca: Emotion driven monocular face capture and animation. In *Proceedings of the IEEE/CVF Conference on Computer Vision and Pattern Recognition*. 20311–20322.

[8] Jiankang Deng, Jia Guo, Niannan Xue, and Stefanos Zafeiriou. 2019. Arcface: Additive angular margin loss for deep face recognition. In *Proceedings of the IEEE/CVF conference on computer vision and pattern recognition*. 4690–4699.

[9] Brecht Desplanques, Jenthe Thienpondt, and Kris Demuynck. 2020. ECAPA-TDNN: Emphasized Channel Attention, Propagation and Aggregation in TDNN Based Speaker Verification. (2020).

[10] Xingping Dong and Jianbing Shen. 2018. Triplet loss in siamese network for object tracking. In *Proceedings of the European conference on computer vision (ECCV)*. 459–474.

[11] Chenpeng Du, Qi Chen, Tianyu He, Xu Tan, Xie Chen, Kai Yu, Sheng Zhao, and Jiang Bian. 2023. DAE-Talker: High Fidelity Speech-Driven Talking Face Generation with Diffusion Autoencoder. *Proceedings of the 31th ACM International Conference on Multimedia (ACM MM)* (2023).

[12] Chenpeng Du, Yiwei Guo, Feiyu Shen, Zhijun Liu, Zheng Liang, Xie Chen, Shuai Wang, Hui Zhang, and Kai Yu. 2024. UniCATS: A unified context-aware text-to-speech framework with contextual vq-diffusion and vocoding. In *Proceedings of the AAAI Conference on Artificial Intelligence*, Vol. 38. 17924–17932.

[13] Yingruo Fan, Zhaojiang Lin, Jun Saito, Wenping Wang, and Taku Komura. 2022. Faceformer: Speech-driven 3d facial animation with transformers. In *Proceedings of the IEEE/CVF Conference on Computer Vision and Pattern Recognition (CVPR)*.

[14] Yao Feng, Haiwen Feng, Michael J Black, and Timo Bolkart. 2021. Learning an animatable detailed 3D face model from in-the-wild images. *ACM Transactions on Graphics (ToG)* 40, 4 (2021), 1–13.

[15] Alex Graves and Alex Graves. 2012. Long short-term memory. *Supervised sequence labelling with recurrent neural networks* (2012), 37–45.

[16] Anmol Gulati et al. 2020. Conformer: Convolution-augmented transformer for speech recognition. *Conference of the International Speech Communication Association (InterSpeech)* (2020).

[17] Yuwei Guo, Ceyuan Yang, Anyi Rao, Yaohui Wang, Yu Qiao, Dahua Lin, and Bo Dai. 2023. Animatediff: Animate your personalized text-to-image diffusion models without specific tuning. *The International Conference on Learning Representations (ICLR)* (2023).

[18] Tianyu He, Junliang Guo, Runyi Yu, Yuchi Wang, Jialiang Zhu, Kaikai An, Leyi Li, Xu Tan, Chunyu Wang, Han Hu, HsiangTao Wu, Sheng Zhao, and Jiang Bian. 2024. GAIA: Zero-shot Talking Avatar Generation.

[19] Jonathan Ho, Ajay Jain, and Pieter Abbeel. 2020. Denoising diffusion probabilistic models. *Advances in neural information processing systems* (2020).

[20] Wei-Ning Hsu, Benjamin Bolte, Yao-Hung Hubert Tsai, Kushal Lakhotia, Ruslan Salakhutdinov, and Abdelrahman Mohamed. 2021. Hubert: Self-supervised speech representation learning by masked prediction of hidden units. *IEEE/ACM Transactions on Audio, Speech, and Language Processing (TASLP)* (2021).

[21] Li Hu, Xin Gao, Peng Zhang, Ke Sun, Bang Zhang, and Liefeng Bo. 2023. Animate anyone: Consistent and controllable image-to-video synthesis for character animation. *arXiv preprint arXiv:2311.17117* (2023).

[22] Haibo Jin, Shengcai Liao, and Ling Shao. 2021. Pixel-in-pixel net: Towards efficient facial landmark detection in the wild. *International Journal of Computer Vision* 129, 12 (2021), 3174–3194.

[23] Diederik P Kingma and Max Welling. 2013. Auto-encoding variational bayes. *arXiv preprint arXiv:1312.6114* (2013).

[24] Tsung-Yi Lin, Piotr Dollár, Ross Girshick, Kaiming He, Bharath Hariharan, and Serge Belongie. 2017. Feature pyramid networks for object detection. In *Proceedings of the IEEE conference on computer vision and pattern recognition*. 2117–2125.

[25] Tao Liu, Chenpeng Du, Shuai Fan, Feilong Chen, and Kai Yu. 2024. DiffDub: Person-Generic Visual Dubbing Using Inpainting Renderer with Diffusion Auto-Encoder. In *ICASSP 2024-2024 IEEE International Conference on Acoustics, Speech and Signal Processing (ICASSP)*. IEEE, 3630–3634.

[26] Ziwei Liu, Ping Luo, Xiaogang Wang, and Xiaoou Tang. 2015. Deep Learning Face Attributes in the Wild. In *Proceedings of International Conference on Computer Vision (ICCV)*.

[27] Yifeng Ma, Shiwei Zhang, Jiayu Wang, Xiang Wang, Yingya Zhang, and Zhidong Deng. 2023. Dreamtalk: When expressive talking head generation meets diffusion probabilistic models. *arXiv preprint arXiv:2312.09767* (2023).

[28] Zhiyuan Ma, Xiangyu Zhu, Guojun Qi, Chen Qian, Zhaoxiang Zhang, and Zhen Lei. 2024. DiffSpeaker: Speech-Driven 3D Facial Animation with Diffusion Transformer. *arXiv preprint arXiv:2402.05712* (2024).

[29] Soumik Mukhopadhyay, Saksham Suri, Ravi Teja Gadde, and Abhinav Shrivastava. 2024. Diff2lip: Audio conditioned diffusion models for lip-synchronization. In *Proceedings of the IEEE/CVF Winter Conference on Applications of Computer Vision*. 5292–5302.

[30] Arsha Nagrani, Joon Son Chung, and Andrew Zisserman. 2017. Voxceleb: a large-scale speaker identification dataset. *arXiv preprint arXiv:1706.08612* (2017).

[31] Youxin Pang, Yong Zhang, Weize Quan, Yanbo Fan, Xiaodong Cun, Ying Shan, and Dong-ming Yan. 2023. Dpe: Disentanglement of pose and expression for general video portrait editing. In *Proceedings of the IEEE/CVF Conference on Computer Vision and Pattern Recognition*. 427–436.

[32] Inkyu Park and Jaewoong Cho. 2023. SAiD: Speech-driven Blendshape Facial Animation with Diffusion. *arXiv preprint arXiv:2401.08655* (2023).

[33] Se Jin Park, Minsu Kim, Jeongsoo Choi, and Yong Man Ro. 2024. Exploring Phonetic Context-Aware Lip-Sync for Talking Face Generation. In *ICASSP 2024-2024 IEEE International Conference on Acoustics, Speech and Signal Processing (ICASSP)*. IEEE, 4325–4329.

[34] Ziqiao Peng, Haoyu Wu, Zhenbo Song, Hao Xu, Xiangyu Zhu, Jun He, Hongyan Liu, and Zhaoxin Fan. 2023. Emotalk: Speech-driven emotional disentanglement for 3d face animation. In *Proceedings of the IEEE/CVF International Conference on Computer Vision*. 20687–20697.

[35] Deepika Phutela. 2015. The importance of non-verbal communication. *IUP Journal of Soft Skills* 9, 4 (2015), 43.

[36] KR Prajwal et al. 2020. A lip sync expert is all you need for speech to lip generation in the wild. In *Proceedings of the 28th ACM international conference on multimedia (ACM MM)*.

[37] Konpat Preechakul et al. 2022. Diffusion Autoencoders: Toward a Meaningful and Decodable Representation. In *IEEE Conference on Computer Vision and Pattern Recognition (CVPR)*.

[38] Yi Ren, Chenxu Hu, Xu Tan, Tao Qin, Sheng Zhao, Zhou Zhao, and Tie-Yan Liu. 2020. Fastspeech 2: Fast and high-quality end-to-end text to speech. *arXiv preprint arXiv:2006.04558* (2020).

[39] Robin Rombach, Andreas Blattmann, Dominik Lorenz, Patrick Esser, and Björn Ommer. 2022. High-resolution image synthesis with latent diffusion models. In *Proceedings of the IEEE/CVF conference on computer vision and pattern recognition*. 10684–10695.

[40] Shuai Shen, Wenliang Zhao, Zibin Meng, Wanhua Li, Zheng Zhu, Jie Zhou, and Jiwen Lu. 2023. DiffTalk: Crafting Diffusion Models for Generalized Audio-Driven Portraits Animation. In *Proceedings of the IEEE/CVF Conference on Computer Vision and Pattern Recognition (CVPR)*.

[41] Aliaksandr Siarohin, Stéphane Lathuilière, Sergey Tulyakov, Elisa Ricci, and Nicu Sebe. 2019. First order motion model for image animation. *Advances in neural information processing systems* 32 (2019).

[42] Jiaming Song, Chenlin Meng, and Stefano Ermon. 2020. Denoising Diffusion Implicit Models. In *International Conference on Learning Representations (ILCR)*.

[43] Michał Stypułkowski, Konstantinos Vougioukas, Sen He, Maciej Zięba, Stavros Petridis, and Maja Pantic. 2024. Diffused heads: Diffusion models beat gans on talking-face generation. In *Proceedings of the IEEE/CVF Winter Conference on Applications of Computer Vision*. 5091–5100.

[44] Jiale Tao, Biao Wang, Tiezheng Ge, Yuning Jiang, Wen Li, and Lixin Duan. 2022. Motion Transformer for Unsupervised Image Animation. In *European Conference on Computer Vision*. Springer, 702–719.

[45] Linrui Tian, Qi Wang, Bang Zhang, and Liefeng Bo. 2024. EMO: Emote Portrait Alive - Generating Expressive Portrait Videos with Audio2Video Diffusion Model under Weak Conditions. arXiv:2402.17485 [cs.CV]

[46] Feng Wang, Jian Cheng, Weiyang Liu, and Haijun Liu. 2018. Additive margin softmax for face verification. *IEEE Signal Processing Letters* 25, 7 (2018), 926–930.

[47] Suzhen Wang, Lincheng Li, Yu Ding, Changjie Fan, and Xin Yu. 2021. Audio2head: Audio-driven one-shot talking-head generation with natural head motion. *International Joint Conference on Artificial Intelligence (IJCAI)* (2021).

[48] Ting-Chun Wang, Arun Mallya, and Ming-Yu Liu. 2021. One-shot free-view neural talking-head synthesis for video conferencing. In *Proceedings of the IEEE/CVF conference on computer vision and pattern recognition*. 10039–10049.

[49] Yaohui Wang, Di Yang, Francois Bremond, and Antitza Dantcheva. 2022. Latent image animator: Learning to animate images via latent space navigation. *Proceedings of the International Conference on Learning Representations* (2022).

[50] Zhou Wang, Alan C Bovik, Hamid R Sheikh, and Eero P Simoncelli. 2004. Image quality assessment: from error visibility to structural similarity. *IEEE transactions on image processing* 13, 4 (2004), 600–612.

[51] Olivia Wiles, A Koepke, and Andrew Zisserman. 2018. X2face: A network for controlling face generation using images, audio, and pose codes. In *Proceedings of the European conference on computer vision (ECCV)*. 670–686.

[52] Liangbin Xie, Xintao Wang, Honglun Zhang, Chao Dong, and Ying Shan. 2022. Vfhq: A high-quality dataset and benchmark for video face super-resolution. In *Proceedings of the IEEE/CVF Conference on Computer Vision and Pattern Recognition*. 657–666.

[53] Shu-wen Yang, Po-Han Chi, Yung-Sung Chuang, Cheng-I Jeff Lai, Kushal Lakhotia, Yist Y Lin, Andy T Liu, Jiatong Shi, Xuankai Chang, Guan-Ting Lin, et al. 2021. Superb: Speech processing universal performance benchmark. *Conference of the International Speech Communication Association (InterSpeech)* (2021).

[54] Bohan Zeng, Xuhui Liu, Sicheng Gao, Boyu Liu, Hong Li, Jianzhuang Liu, and Baochang Zhang. 2023. Face Animation with an Attribute-Guided Diffusion Model. In *Proceedings of the IEEE/CVF Conference on Computer Vision and Pattern Recognition*. 628–637.

[55] Chenxu Zhang, Chao Wang, Jianfeng Zhang, Hongyi Xu, Guoxian Song, You Xie, Linjie Luo, Yapeng Tian, Xiaohu Guo, and Jiashi Feng. 2023. DREAM-Talk: Diffusion-based Realistic Emotional Audio-driven Method for Single Image Talking Face Generation. *arXiv preprint arXiv:2312.13578* (2023).

[56] Richard Zhang, Phillip Isola, Alexei A Efros, Eli Shechtman, and Oliver Wang. 2018. The unreasonable effectiveness of deep features as a perceptual metric. In *Proceedings of the IEEE conference on computer vision and pattern recognition (CVPR)*.

[57] Wenxuan Zhang, Xiaodong Cun, Xuan Wang, Yong Zhang, Xi Shen, Yu Guo, Ying Shan, and Fei Wang. 2023. SadTalker: Learning Realistic 3D Motion Coefficients for Stylized Audio-Driven Single Image Talking Face Animation. In *Proceedings of the IEEE/CVF Conference on Computer Vision and Pattern Recognition*. 8652–8661.

[58] Zhimeng Zhang et al. 2023. DINet: Deformation Inpainting Network for Realistic Face Visually Dubbing on High Resolution Video. *Thirty-Seventh AAAI Conference on Artificial Intelligence (AAAI)* (2023).

[59] Zhimeng Zhang, Lincheng Li, Yu Ding, and Changjie Fan. 2021. Flow-guided one-shot talking face generation with a high-resolution audio-visual dataset. In *Proceedings of the IEEE/CVF Conference on Computer Vision and Pattern Recognition (CVPR)*.

[60] Weizhi Zhong, Chaowei Fang, Yinqi Cai, Pengxu Wei, Gangming Zhao, Liang Lin, and Guanbin Li. 2023. Identity-Preserving Talking Face Generation with Landmark and Appearance Priors. In *Proceedings of the IEEE/CVF Conference on Computer Vision and Pattern Recognition (CVPR)*.

[61] Hang Zhou, Yasheng Sun, Wayne Wu, Chen Change Loy, Xiaogang Wang, and Ziwei Liu. 2021. Pose-controllable talking face generation by implicitly modularized audio-visual representation. In *Proceedings of the IEEE/CVF conference on computer vision and pattern recognition (CVPR)*.

[62] Yang Zhou, Xintong Han, Eli Shechtman, Jose Echevarria, Evangelos Kalogerakis, and Dingzeyu Li. 2020. Makelttalk: speaker-aware talking-head animation. *ACM Transactions On Graphics (TOG)* (2020).

# A DATA PROCESSING PIPELINE

Our data collection pipeline contains in four distinct stages, utilizing the datasets VoxCeleb [30], HDTF [59], and VFHQ [52]:

(1) **Re-downloading Original Datasets**: To ensure uniform processing, given the different data handling methods across datasets, we downloaded the original videos. For VoxCeleb and HDTF, changes in the original sources meant we could only secure about 60-70% of the initial datasets. The VFHQ authors provided the complete set of videos, obviating the need for re-downloading.

(2) **Face Detection**: This step involves detecting faces in videos. In contrast to previous studies, we chose not to align the faces to allow for positional shifts within the frame, aiming to preserve natural head movements.

(3) **Applying Filtering Rules**: Our filtering process involved two main criteria. We first excluded faces with resolutions lower than $256 \times 256$. Then, we conducted blur detection using the Laplacian operator and angle detection, excluding faces with a yaw angle greater than 60 degrees.

(4) **Selecting Video Clips Based on Identity ID Tags**: To ensure a diversity of identities for the robust training of the identity encoder, we randomly selected 2-3 video clips per ID.

(5) **Resize to $256 \times 256$**: All our images, whether for training or testing, are originally based on the resolution of $256 \times 256$. Therefore, the purpose of this step is to resize all images to $256 \times 256$.

Finally, our efforts yielded a dataset containing 4,242 unique speaker IDs, encompassing a total of 17,108 video clips with a cumulative duration of 55 hours. Additionally, since the VFHQ dataset lacks an audio track, it was used exclusively during the motion representation training phase.

Table 5 provides comparative metrics of our dataset against those of EMO [45] and GAIA [18]. As outlined in the table, our dataset contains roughly a quarter of the unique human identifiers found in GAIA and about one-fifth of the training hours compared to EMO. Furthermore, our algorithm can be trained from scratch and does not rely on parameter initialization.

# B TRAINING DETAILS

## B.1 Data Augmentation

For source and target images, no data augmentation strategies can be applied. The objective of this constraint is to ensure the consistency of the background, allowing the motion latent space to capture human motion without background movement. However, when training the identity encoder using metric learning, it becomes necessary to introduce some negative candidates. At this point, we can employ standard augmentation techniques, which include horizontal flipping, color jitter, Gaussian blur, shifting, scaling, and rotation. The specific implementations of these techniques are facilitated by the tools available at this URL [3].

**Table 5: Comparison of training dataset statistics. "#IDs": Number of unique human identifiers. "#Clips": Total number of video segments. "Hours": Total training hours. "TFS": Training from scratch. "-" indicates that this information is not provided.**

| Method | #IDs | #Clips | Hours | TFS |
|---|---|---|---|---|
| GAIA [18] | 15,969 | - | 1,169 | ✓ |
| EMO [45] | - | - | 250 | ✗ |
| **AniTalker** | 4,242 | 17,108 | 55 | ✓ |

## B.2 Training Configuration

*B.2.1 Training Loss.* **Metric Learning Loss** For the Triplet Loss [10], we set the margin to 0.01 and use the L2 distance metric. For the angular additive margin softmax (AAMSoftmax [46]), we set the margin $m$ to 0.2 and the scaling factor $s$ to 30, utilizing cosine distance.

**Mutual Information Decoupling Loss** We use the Contrastive Log-ratio Upper Bound (CLUB) [4] for mutual information (MI) minimization in high-dimensional spaces where only samples are available, not distribution forms. CLUB uses contrastive learning to estimate MI by contrasting conditional probabilities between positive and negative sample pairs. A variational form of CLUB (vCLUB) is developed for scenarios where the conditional distribution $p(y|x)$ is unknown, using a neural network to approximate $p(y|x)$. CLUB is further accelerated using a negative sampling strategy, enhancing computational efficiency while maintaining reliable MI estimation capabilities. Details can be found in this repo [4]. Here, we use the CLUB estimator to measure the differences between identity and motion distributions and minimize them.

**Loss for Training Motion Representation** This is also our primary loss function for training the motion encoder during the first phase. We utilize various types of losses, mainly comprising losses related to reconstruction (reconstruction loss $L_{recon}$, perceptual loss $L_{percep}$), adversarial loss ($L_{adv}$), mutual information loss ($L_{MI}$), and identity metric learning loss ($L_{ML}$). The specific forms of the reconstruction, perceptual, and adversarial losses are consistent with those used in LIA [49]. The overall loss is a weighted sum of these individual losses, as shown below:

$$L_{motion} = L_{recon} + \lambda_1 L_{percep} + \lambda_2 L_{adv} + \lambda_3 L_{MI} + \lambda_4 L_{ML}$$

where the values of $\lambda_1$, $\lambda_2$, $\lambda_3$, and $\lambda_4$ are 0.1, 1, 0.1, and 0.1 respectively, in our experiment.

**Loss for Training Motion Generator** In our model, the generation loss

$$L_{\text{gen}} = L_{\text{diff}} + \lambda \sum_{k=1}^{K} L_{\text{var}_k}$$

is structured around two sets of attributes (i.e., $K = 2$). The first set pertains to camera parameters, including the position of the face within the frame and the scale of the face. The second set is related to pose attributes, consistent with methods [11, 18]. Specifically, the $L_{\text{var}_k}$ losses are L2 losses between the predicted values and

---

[3] https://github.com/albumentations-team/albumentations

[4] https://github.com/Linear95/CLUB/

the ground truth values. Details regarding the feature extraction and representation for camera parameters and pose will be discussed in the upcoming sections. Additionally, we set $\lambda$ to 1 in this formulation.

For the training of diffusion models, we employed the simplified loss objective described in [19] for the training of DDPMs. During the training phase, we used 1000 timesteps, while in the inference stage, we utilized DDIM [42] acceleration with 50 timesteps. We did not employ additional performance-enhancing methods such as class-free guidance (CFG).

*B.2.2 Training and Inference Hardware.* For training, we utilized four A100 (40G) GPUs, training each phase until the loss converged. Besides computing the perceptual loss, we did not incorporate any pre-trained parameters. The first phase, focusing on motion representation training, converged relatively quickly, requiring approximately 50 hours. The second phase, where we employed an exponential moving average (EMA) to stabilize training, converged more slowly, taking about 120 hours. For inference, we utilized a GeForce RTX 3060 Ti (8G) GPU. The process begins by generating a motion sequence from audio, followed by frame-by-frame rendering, which can support up to several minutes of inference without triggering memory overflow errors. Specifically, the GPU with 8G VRAM can generate up to 3 minutes of video in one inference.
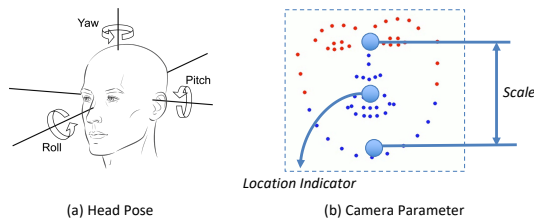


**Figure 8: Controllable Attribute Features: Head Pose and Camera Parameter**

*B.2.3 Controllable Attribute Features.* We utlize two types of features for controlling talking face generation. The first is the head pose, which includes yaw, pitch, and roll information, utilizing these three degrees of freedom to control the head's orientation, consistent with approaches found in [18, 37]. We use a pretrained extraction network[5] to derive these three-dimensional features. Additionally, to further capture the facial variations within the frame, we considered two parameters: the face's position in the frame and its size, which indicates the distance from the camera. These parameters are defined as camera parameters. Specifically, for the face's position, we use the x-coordinate of the nose landmark, as we observed that the face mostly moves horizontally rather than vertically. For the face's scale, we measure the distance from the eyebrows to the chin. These two attributes form a two-dimensional camera parameter feature. The visualization is illustrated in Figure 8.

Overall, during the training phase, we utilize several pre-trained models as attribute extractors for three attributes: head pose, head location, and head scale. In actual inference, since these features

[5]https://github.com/cleardusk/3DDFA_V2

are explicit and interpretable, we can directly input specific values to control aspects such as the pitch angle, which can range from -90 to 90 degrees, to simulate head movements like nodding or looking up.

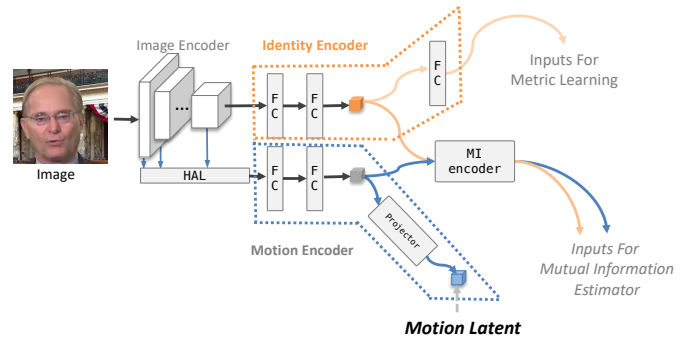## C MODEL DETAILS

### C.1 Identity and Motion Encoder



**Figure 9: Detailed structure of the motion latent extraction**

This section details the structures of the motion and identity encoders used during the first phase of training motion representations, as illustrated in Figure 9. The identity encoder is designed to learn identity information, with its outputs directed through a series of fully connected layers to a metric learning loss. Conversely, the motion encoder focuses on learning motion encoding, with its outputs routed to a loss function that calculates mutual information. This output later serves as an input for rendering and for generating results in the second phase. To reduce the dimensionality of the motion encoding and ensure a more compact representation, an additional projector is used, as indicated in the diagram. We tested two types of projectors: (1) **Direct Reduction**, which uses an FC layer to reduce the dimensionality of the hidden layer from 512 to a target dimension of 20, as depicted in the figure. (2) **Linear Motion Decomposition** [49], a method that represents motion in latent space by learning a set of orthogonal bases, each vector representing a fundamental visual transformation. The term "20 dimensions" refers to the number of distinct axes or directions in this space, which can be manipulated to encode different types of motion or transformations. In our experiments, we opted for the LMD approach. Comparative analysis and further discussion are presented in Section C.4.2.

### C.2 Rendering Block

In our Rendering Block, we utilize the design of the G block from LIA [49], a wrap-based rendering module responsible for handling motion and features from different layers of the image encoder (derived from a portrait). This module samples the features, as depicted in the simplified structure in Figure 10. Here, the motion features generate a flow field that performs a wrap operation, creating deformed features based on features from layer i. These deformed features are then combined with a mask through dot product operations to restrict specific regions, followed by a toRGB conversion

**Table 6: Model Configuration on Speech Encoder (SE) and Diffusion Motion Generator (DMG)**

| Config. | SE | DMG |
|---|---|---|
| attention_dim | 512 | 1024 |
| attention_heads | 2 | 2 |
| # layers | 4 | 2 |
| dropout_rate | 20% | 20% |
| # params (M) | 13 | 25 |
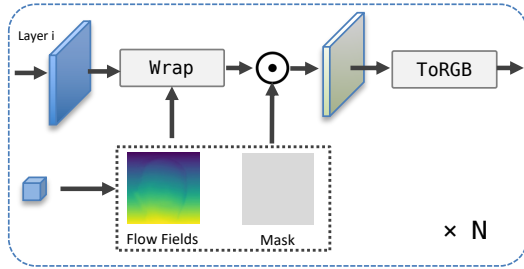


**Figure 10: Rendering Block**

to produce the image. This module is executed N times, where N corresponds to the number of layers in the image encoder. In our experiments, we used N=8, with the width and height of the feature map from layer 1 to layer 8 being $256 \times 256$, $128 \times 128$, $64 \times 64$, $32 \times 32$, $16 \times 16$, $8 \times 8$, $4 \times 4$, and $1 \times 1$ respectively.

## C.3 Motion Generator

The motion generator aims to convert an audio input and a portrait into a motion sequence, which is then rendered by the image decoder. The main trainable modules involved are the speech encoder, variance adapter, and diffusion motion generator, which together create the motion latent. Both the speech encoder and the diffusion motion generator use the Conformer [16][6], with configuration details presented in Table 6.

The speech encoder processes downsampled audio features with dimensions $T \times C_1$, where $C_1$ is 512. Additionally, the input to the Diffusion Motion Generator consists of multiple components, formed by concatenating outputs from the speech encoder, the start motion latent and feature of the portrait, noisy latent, and time embedding. The start motion latent and feature of the portrait refer to the results of the portrait image encoder and the motion latent, respectively, with dimensions $T \times C_2$ and $T \times C_3$, where $C_2$ and $C_3$ are 512 and 20 in our experiments. The noisy latent is the noise-augmented motion latent with dimensions $T \times C_3$, and the time embedding is the diffusion time condition with dimensions $T \times 1$. These dimensions, except for the speech encoder, are unified to $T \times 128$ when input into the model. Ultimately, the Diffusion Motion Generator's input includes a 1024-dimensional vector comprising the speech encoder's input (512 dimensions), the start motion latent (128 dimensions), the start feature (128 dimensions), noisy latent (128 dimensions), and time embedding (128 dimensions).

**Table 7: Comparison on the Capabilities of the Human Face Renderer**

| Method | Renderer | # params (M) | PSNR ↑ | SSIM↑ |
|---|---|---|---|---|
| GAIA [18] | VAE[7] | 50 | 30.497 | 0.924 |
| EMO [45] | VAE[8] | 84 | 33.114 | 0.960 |
| **AniTalker** | Wrap-based | 50 | 35.634 | 0.979 |

**Table 8: Parameter search on the projector of the motion encoder**

| Method | FC | LMD | Dim. | PNSR ↑ | SSIM ↑ | LPIPS ↓ | CSIM↑ |
|---|---|---|---|---|---|---|---|
| AniTalker | ✓ | | 32 | 28.653 | 0.899 | 0.081 | 0.924 |
| | | ✓ | 32 | 29.204 | 0.905 | 0.079 | 0.927 |
| | ✓ | | 20 | 28.387 | 0.895 | 0.083 | 0.922 |
| | | ✓ | 20 | 29.071 | 0.905 | 0.079 | 0.927 |
| | ✓ | | 10 | 27.685 | 0.879 | 0.089 | 0.914 |
| | | ✓ | 10 | 27.999 | 0.892 | 0.086 | 0.920 |

The model parameters for the speech encoder, variance adapter, and diffusion motion generator are 13M, 2M, and 25M respectively, totaling 40M parameters for the motion generator stage.

## C.4 Experiments

*C.4.1 Analysis on Image Renderer.* To compare rendering capabilities across different methods, we conducted a comparison with GAIA [18] and EMO [45], both employing a VAE [23]-based renderer. We randomly selected 100 images from the Celeb-A [26] face dataset to test reconstruction capabilities on human faces by extracting latent representations and then reconstructing based on these representations. For GAIA, since it is not open-sourced and to ensure a fair comparison, we used a structure similar to the one described in their paper and trained it with a model parameter size and dataset identical to our rendering module. Results in the table show that our method outperforms GAIA in facial reconstruction. Additionally, we compared our renderer with EMO's, which adopts the architecture of Stable Diffusion [39]. Despite its larger parameter size, our results also demonstrate improvement in reconstruction. We attribute these outcomes to two main factors: firstly, the VAE-based perceptual compression [39] process tends to lose information, particularly high-frequency details such as hair strands. Secondly, VAEs are generally designed for generic static image generation tasks in Stable Diffusion and are not specifically tailored for representing human faces.

*C.4.2 Analysis on the motion projector.* To evaluate the structure of the motion projector and the impact of varying dimensions, we conducted a parameter search, as detailed in Table 8. First, to verify the effectiveness of Fully Connected (FC) and Linear Motion Decomposition (LMD) [49], we performed comparative experiments. From the table, LMD generally showed more favorable outcomes under any dimensions, which we attribute to its orthogonality. This orthogonality acts as a regularization method, implicitly enforcing

---

[6]https://github.com/espnet/espnet/blob/master/espnet2/asr/encoder/conformer_encoder.py

[7]Our reproduced result

[8]https://huggingface.co/runwayml/stable-diffusion-v1-5

separation between different features and thus enhancing performance.

Furthermore, to assess the impact of dimensionality on the model, we conducted experiments with three sets of dimensions: 10, 20, and 32. As the dimensions increased, the overall performance showed improvement. However, from 20 to 32, there was no significant enhancement, especially for metrics like SSIM, LPIPS, and CSIM, which showed no change. Therefore, all our experiments were based on a dimensionality of 20 combined with the Linear Motion Decomposition strategy.
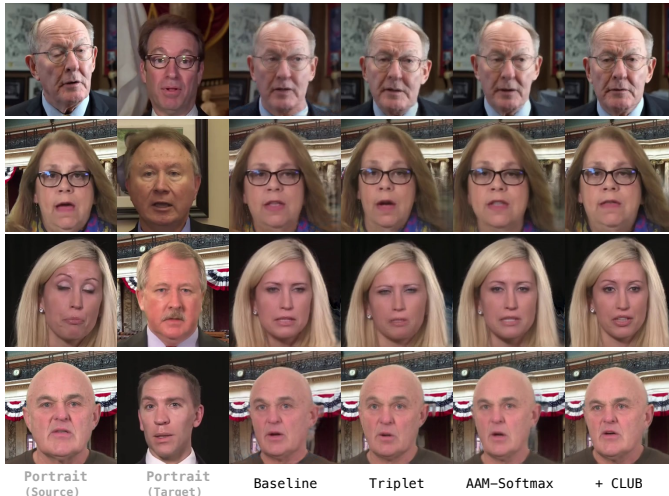


**Figure 11: Visual ablation study of identity and motion disentanglement using different methods.**

*C.4.3  Visual Ablation Study on Disentanglement.* As a supplement to Section 4.4.1 of the main paper, we have randomly visualized several sets of disentanglement results, as illustrated in Figure 11. The objective is to drive the source portrait using the motion of the target portrait. In the absence of any metric learning or mutual information loss constraints, the baseline results exhibit issues of identity leakage, as shown in the third column of the figure. Implementing Euclidean distance metric learning or angle-based metric learning can mitigate the leakage to some extent, but problems still persist, as depicted in columns four and five. Furthermore, by incorporating mutual information loss on top of angle-based metric learning, the leakage issues are significantly alleviated, as demonstrated in the last column of the figure.

## D  DEMO SETUP

To further illustrate the effectiveness of our experiments, we have prepared an extensive set of demonstrations available at AniTalker Project Page [9]. Below, we provide a detailed explanation of the demo page setup:

(1) **Audio-driven Talking Face Generation (Realism):** The input consists of audio plus random noise. The variance

adapter does not receive any control signals, aiming to test the model's capability to generate realistic human faces.

(2) **Audio-driven Talking Face Generation (Statue/Cartoon):** Similar to the realism setup, this demo tests the model with statues, reliefs, and cartoon characters. The results demonstrate our method's strong generalization capabilities.

(3) **Video-driven Talking Face Generation (Cross/Self Reenactment):** To test the reconstruction effectiveness of motion representations, both identity-consistent and cross-identity tests are conducted. Motions from another/same person are used to drive a particular portrait without involving audio.

(4) **Diversity:** To test the impact of diffusion noise on the results, we initially used two different random seeds, followed by nine different random seeds. The results demonstrate that while maintaining the consistency of the generated effects, noise can produce diverse outcomes.

(5) **Controllability:** Testing the controllability of the variance adapter, we examined the results of combined control over pose, head location, and audio.

(6) **Long Video Generation:** For long video generation, two cases are considered. We first generate text with ChatGPT [10], then use Text-to-speech (TTS) [11] to convert them to audio. The reading audio drives the portrait, testing the capability to generate long-duration videos. These videos, lasting several minutes, are generated on a GPU with only 8GB of VRAM (3060Ti), confirming that our algorithm does not rely on extensive computing resources.

(7) **Method Comparison (Audio-driven):** Comparisons are made with baseline methods [47, 57, 61, 62] driven by audio.

(8) **Method Comparison (Video-driven):** Comparisons are made with baseline methods [31, 41, 44, 48, 49, 54] driven by video, specifically comparing face reenactment techniques.

(9) **Ablation Study:** To validate the impact of different modules on the outcomes, we tested four scenarios: mutual information decoupling, comparison with traditional representations, the variance adapter module, and the HAL module.

## E  ETHICAL CONSIDERATION

The potential misuse of lifelike digital human face generation, such as for creating fraudulent identities or disseminating misinformation, necessitates preemptive ethical measures. Before utilizing these models, it is crucial for organizations to integrate ethical guidelines into their policies, ensuring the application of this technology emphasizes consent, transparency, and accountability. Furthermore, it is recommended to embed visible or invisible digital watermarks in any generated content.

---

[9]https://github.com/X-LANCE/AniTalker/

[10]https://chat.openai.com/
[11]https://azure.microsoft.com/